Supplement of The Cryosphere, 11, 1553–1573, 2017
https://doi.org/10.5194/tc-11-1553-2017-supplement

The Cryosphere Open Access EGU

Supplement of

Sea-ice deformation in a coupled ocean–sea-ice model and in satellite remote sensing data

G. Spreen et al.

Correspondence to: Gunnar Spreen (gunnar.spreen@uni-bremen.de)

Sea-Ice Deformation in a Coupled Ocean-Sea Ice Model and in Satellite Remote Sensing Data — Supplementary Material

Gunnar Spreen[1,2], Ron Kwok[2], Dimitris Menemenlis[2], and An T. Nguyen[2,3]

[1]University of Bremen, Institute of Environmental Physics, Bremen, Germany.
[2]Jet Propulsion Laboratory, California Institute of Technology, Pasadena, CA, USA.
[3]now at The University of Texas at Austin, TX, USA.

Correspondence to: Gunnar Spreen (gunnar.spreen@uni-bremen.de)

This document provides some supplementary figures and tables in support of the main text. In the first section S-1 alternative versions of the figures and tables from the main text based on the unfiltered RGPS and model data are presented. All calculations are the same as described in the main text with the sole exception that the anisotropic filter described in Bouillon and Rampal (2015) was not applied. Section S-2 presents more example maps of sea ice divergence, vorticity, and shear.

S-1 Figures and Tables for Unfiltered Data

All figures and tables from the main text, where the filter from Bouillon and Rampal (2015) influences the results, are presented here again without the filter applied. All conclusions from the main text are also valid for the unfiltered results. There are, however, differences in the magnitude and numbers for the sea ice deformation variables and scaling exponents.

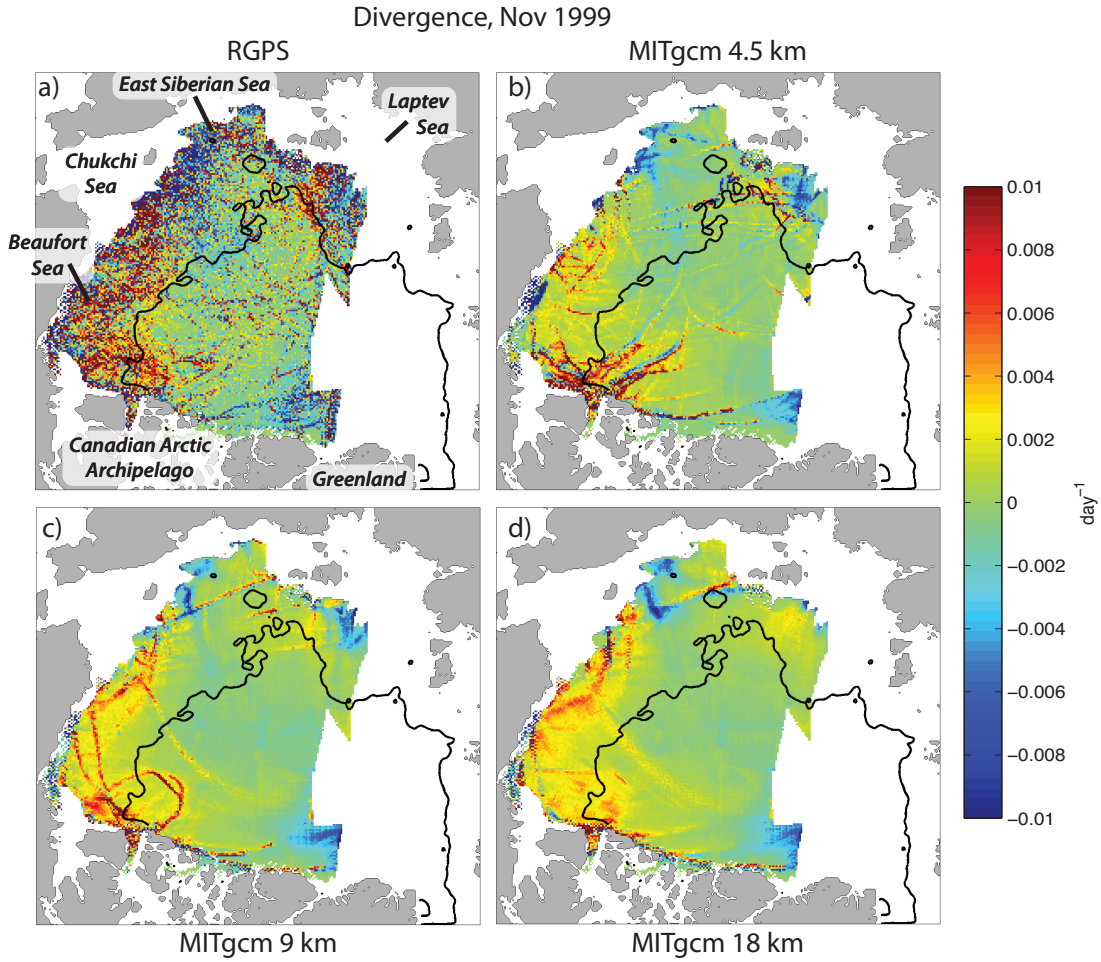

Figure S-1. Examples of monthly mean November 1999 sea ice divergence. The divergence from (a) RGPS and the model runs with (b) 4.5-km, (c) 9-km, and (d) 18-km grid spacing are shown. The number of LKFs increases with decreasing model grid spacing. All maps are shown on the same 12.5 km grid and are constructed from the same number of observations. The black line discriminates seasonal and perennial sea ice. White areas are not covered by RGPS observations.

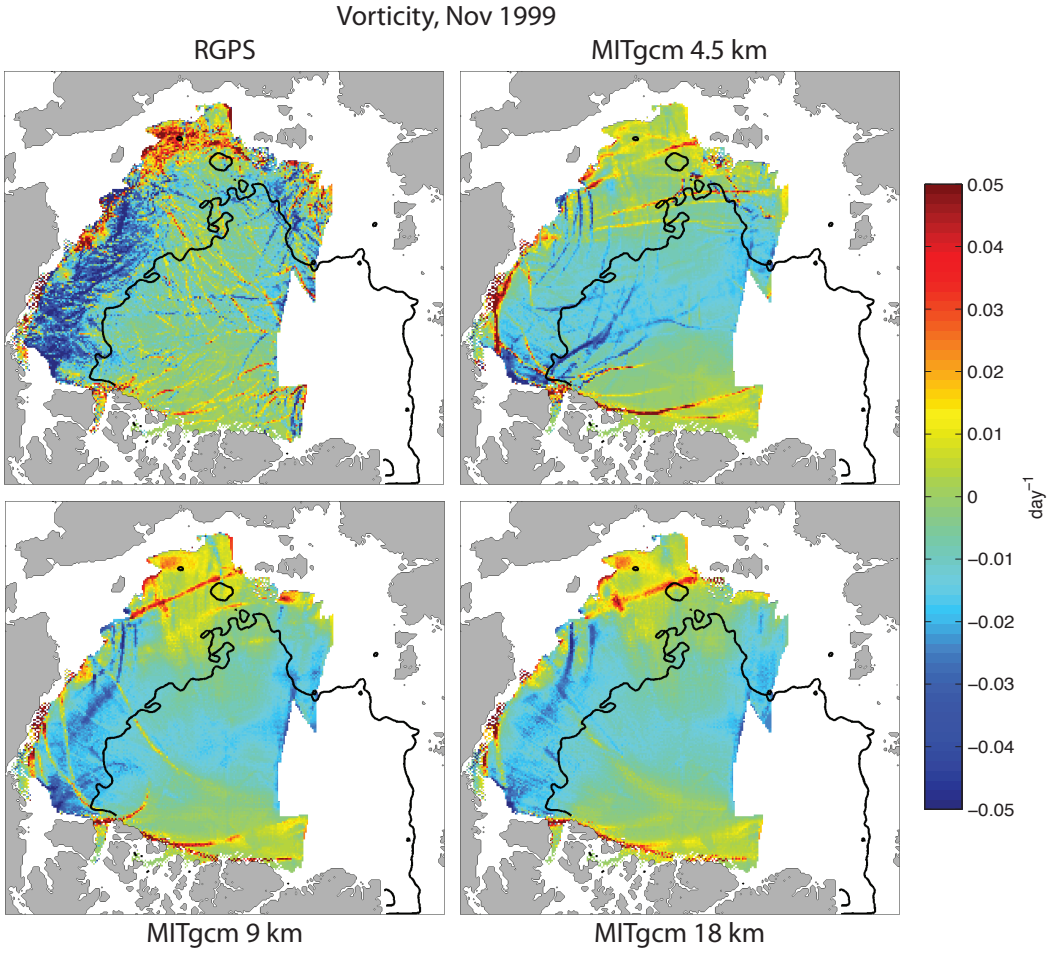

Figure S-2. As Figure S-1 but for vorticity.

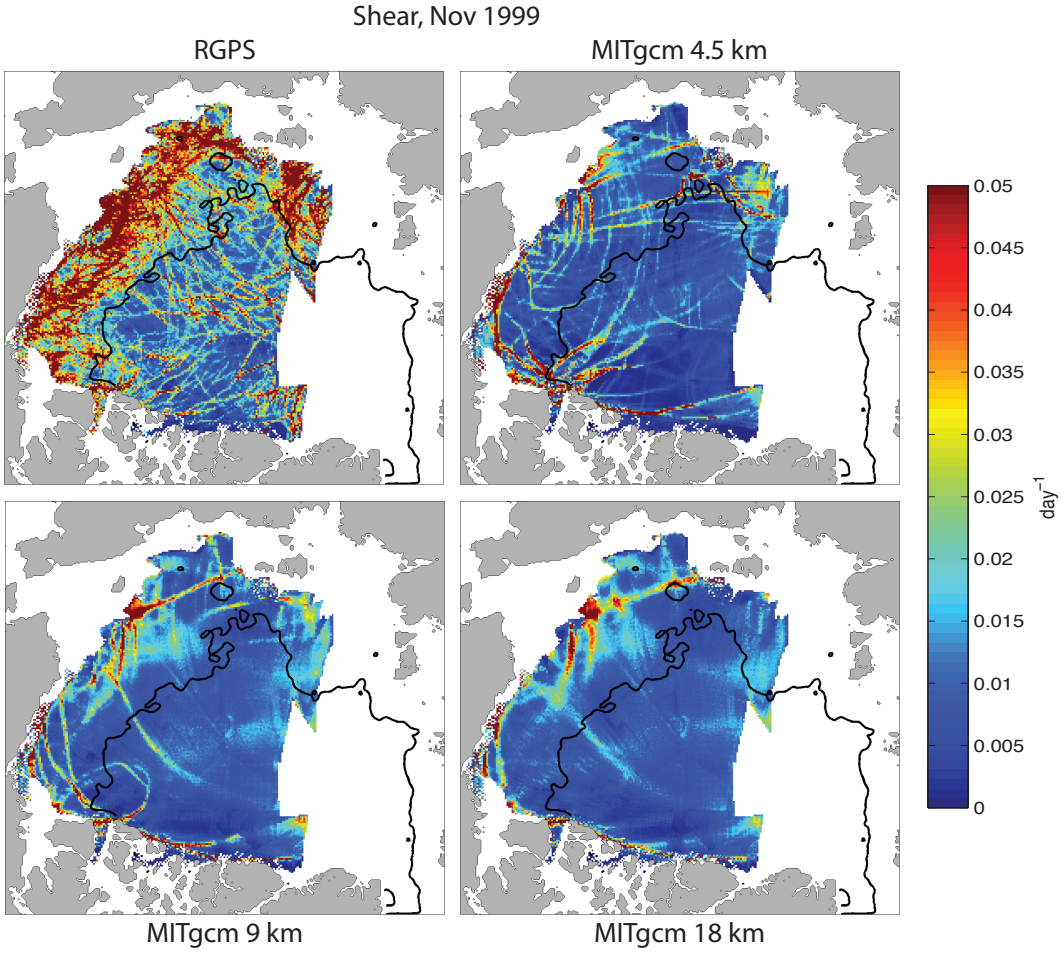

Figure S-3. As Figure S-1 but for shear.

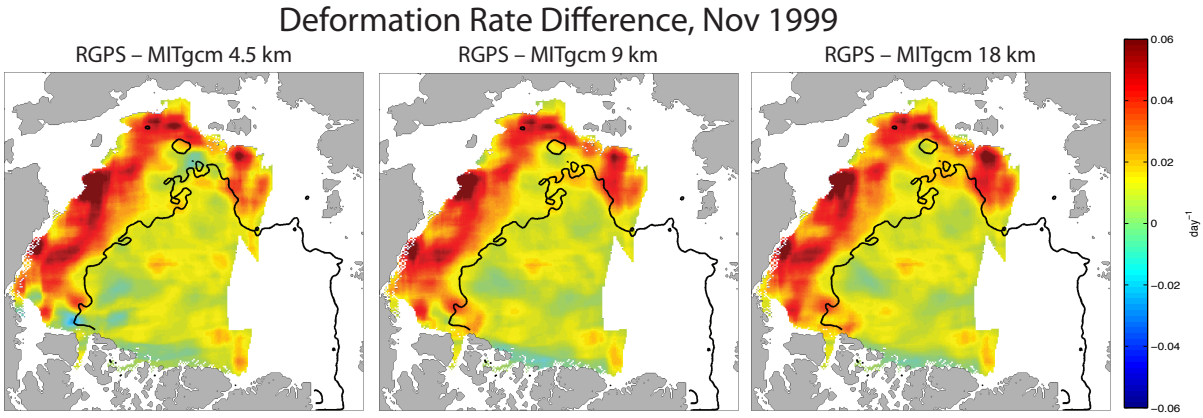

Figure S-4. Smoothed (150 km) difference in deformation rate $\dot{D}$ between RGPS and model solutions with 4.5 km (left), 9 km (middle), and 18 km (right) grid spacing. Largest differences occur in the seasonal ice zone outside the black contour.

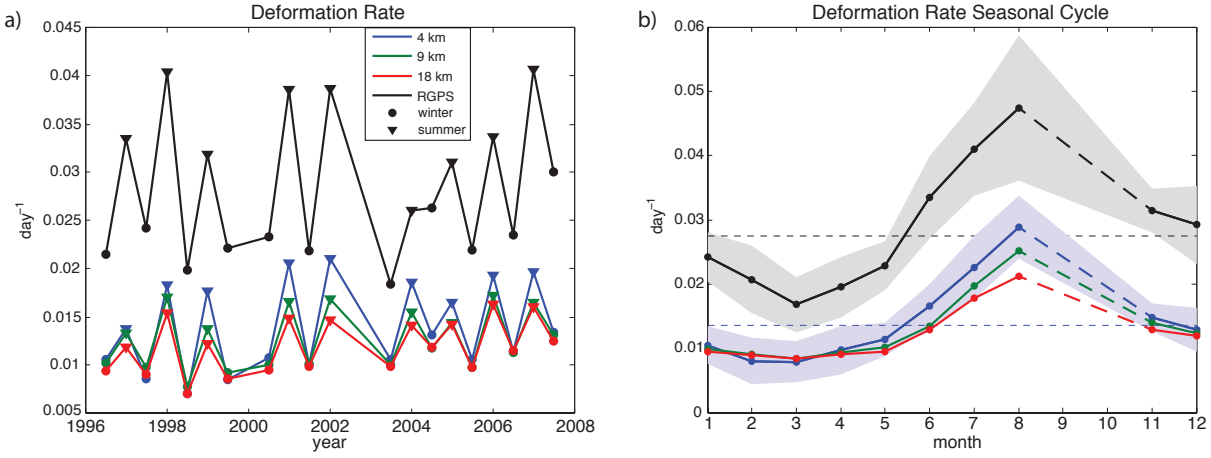

Figure S-5. a) Mean deformation rate $\dot{D}$ for all 20 RGPS periods and the corresponding modeled values. Circles mark winter periods and triangles summer periods; note that periods have different length. b) Seasonal cycle of $\dot{D}$; shaded areas show standard deviations for RGPS and the 4.5-km solution (9 and 18-km solutions are similar); horizontal dashed lines show the mean calculated from the monthly time series; note that no data is available for September and October.

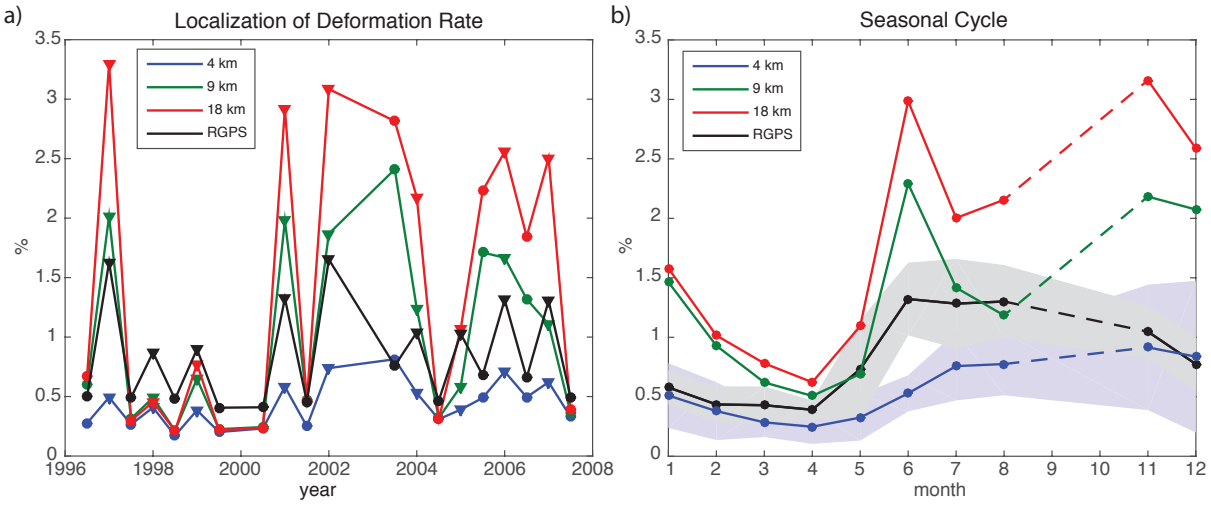

Figure S-6. The percentage Q of area containing the highest 15% of all sea-ice deformation rates shows the localization of deformation. a) Time series showing the absolute percentage Q for RGPS data (black) and model solutions with 4.5 (blue), 9 (green), and 18 km (red) grid spacing for all 20 RGPS periods. Circles mark winter periods and triangles summer periods; note that periods have different length. b) Seasonal cycle of Q; shaded areas show standard deviations for RGPS and the 4.5-km solution (9 and 18-km solutions are similar); note that no data is available for September and October.

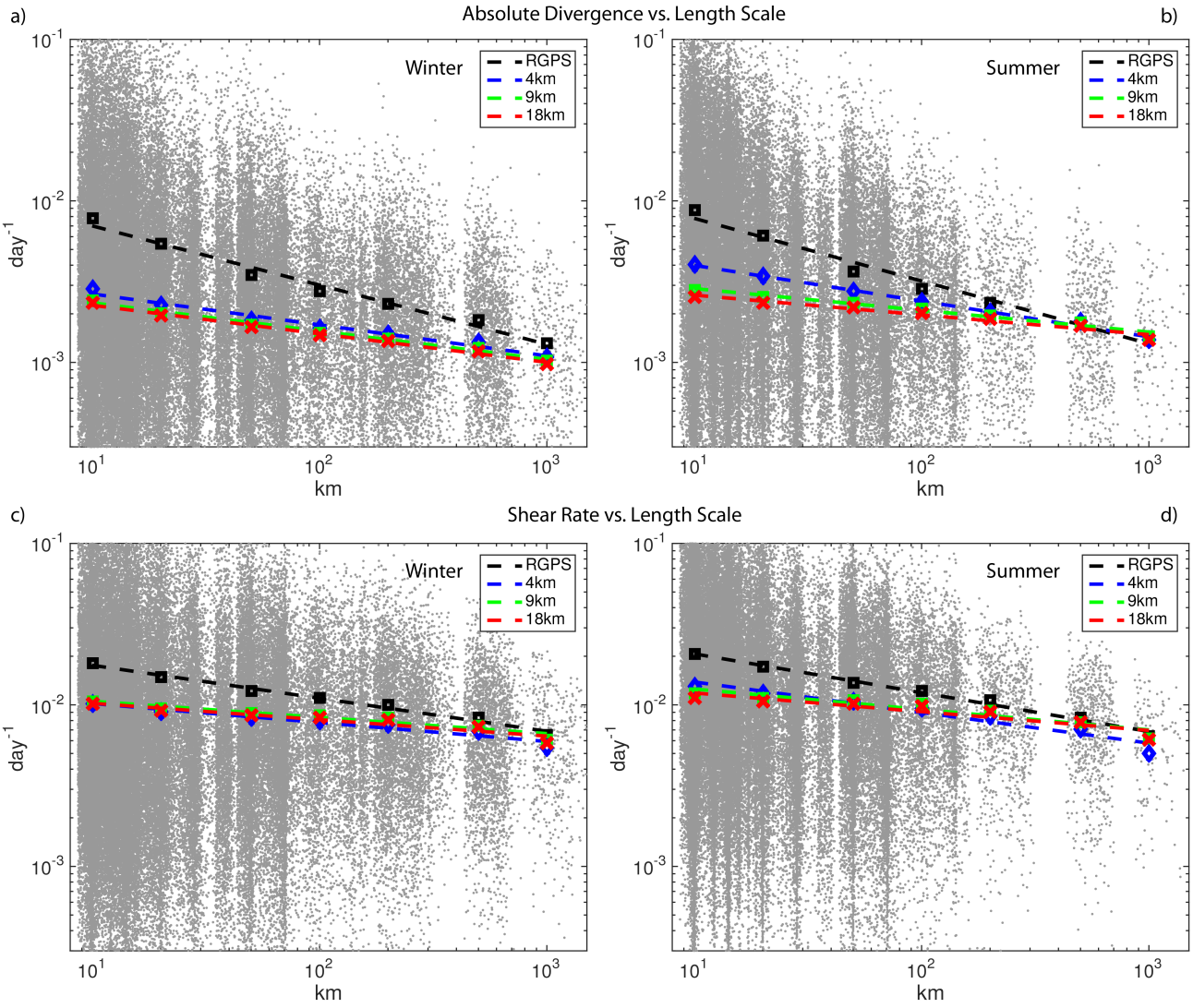

Figure S-7. Scaling properties of absolute sea-ice divergence $|\dot{\nabla}|$ (a, b) and shear rate $\dot{\tau}$ (c, d) for RGPS and model solutions for all winter (Nov–May; a, c) and summer (May–Aug; b, d) periods. For length scales of 10, 20, 50, 100, 200, 500, and 1000 km the ice divergence and shear from the Lagrangian cells were aggregated over 5-day periods. Individual data points for the RGPS dataset are shown in grey. Mean values for the six different length scales are marked with symbols. Dashed lines are least square fits to the six mean values from 10 to 1000 km. Note the logarithmic axes scaling.

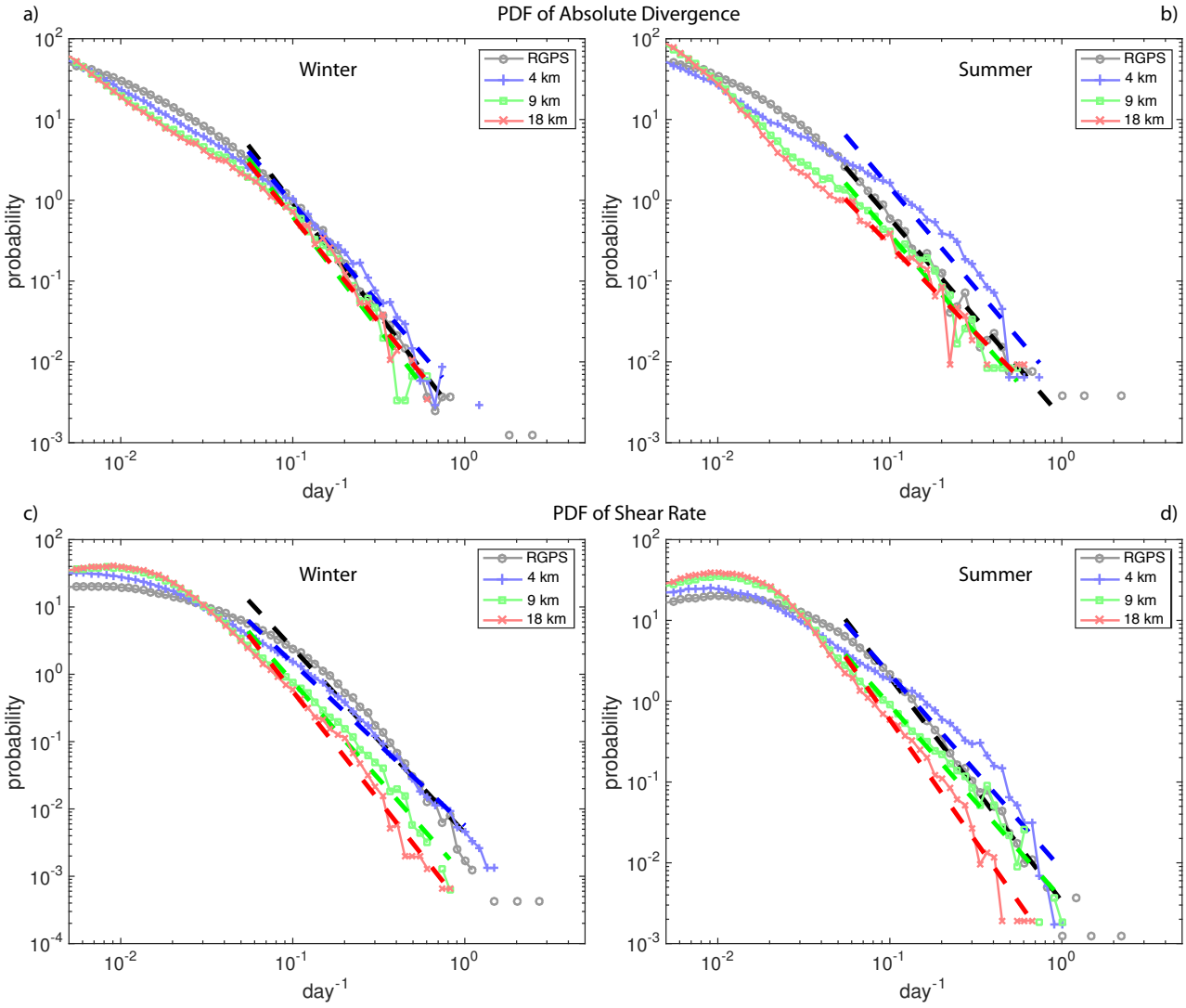

Figure S-8. Probability density function of absolute sea-ice divergence $|\dot{\nabla}|$ (a, b) and shear rate $\dot{\tau}$ (c, d) for a length scale of 20 km based on 5-daily aggregated Lagrangian cells for all winter (Nov–May) and summer (May–Aug) periods for RGPS and model solutions. Dashed lines are least square fits to the approximately linear part of the PDFs between 0.05 and 1.0 day^{-1}. Note the logarithmic axes scaling.

Table S-1. Overview of some statistical parameters for the complete 97-month time series of RGPS and model sea ice strain rate invariants. All units are $10^{-2}\,\mathrm{day}^{-1}$ if not otherwise indicated; $\pm$ values denote the standard deviation of the time series; 'difference' is the difference between model and RGPS in %; and 'correlation' is the correlation coefficient between the model and RGPS time series. The last rows summarize the power-law scaling exponents b and n (plus 95% confidence bounds; no units).

$\cdot 10^{-2}$		RGPS	4.5 km	9 km	18 km
deformation rate $\dot{D}$	mean	2.9 ± 1.1	1.4 ± 0.7	1.4 ± 0.6	1.3 ± 0.5
	difference		-50%	-53%	-56%
	correlation		0.86	0.89	0.87
absolute divergence $\lvert\dot{\nabla}\rvert$	mean	1.2 ± 0.5	0.5 ± 0.3	0.4 ± 0.2	0.4 ± 0.2
	difference		-65%	-72%	-74%
	correlation		0.85	0.83	0.81
absolute vorticity $\lvert\dot{\zeta}\rvert$	mean	2.4 ± 0.7	1.4 ± 0.6	1.4 ± 0.4	1.3 ± 0.4
	difference		-41%	-43%	-46%
	correlation		0.76	0.79	0.77
shear $\dot{\tau}$	mean	2.5 ± 0.9	1.3 ± 0.7	1.3 ± 0.5	1.3 ± 0.5
	difference		-47%	-49%	-52%
	correlation		0.85	0.89	0.88
percentage Q of area	mean	$0.7 \pm 0.4\%$	$0.5 \pm 0.4\%$	$1.2 \pm 1.1\%$	$1.5 \pm 1.4\%$
containing highest 15%	difference		-36%	65%	122%
of deformation rates	correlation		0.59	0.60	0.75
spatial scaling exponent b for	winter	-0.37 ± 0.06	-0.19 ± 0.03	-0.18 ± 0.02	-0.18 ± 0.02
absolute divergence $\lvert\dot{\nabla}\rvert$	summer	-0.38 ± 0.07	-0.22 ± 0.02	-0.13 ± 0.03	-0.12 ± 0.03
spatial scaling exponent b for	winter	-0.20 ± 0.03	-0.12 ± 0.04	-0.10 ± 0.03	-0.10 ± 0.04
shear $\dot{\tau}$	summer	-0.24 ± 0.02	-0.19 ± 0.06	-0.13 ± 0.05	-0.12 ± 0.06
spatial scaling exponent b for	winter	-0.22 ± 0.03	-0.12 ± 0.04	-0.11 ± 0.03	-0.11 ± 0.04
deformation rate $\dot{D}$	summer	-0.25 ± 0.02	-0.19 ± 0.05	-0.13 ± 0.05	-0.12 ± 0.05
PDF scaling exponent n for	winter	-2.76 ± 0.06	-2.5 ± 0.1	-2.8 ± 0.1	-2.60 ± 0.09
absolute divergence $\lvert\dot{\nabla}\rvert$	summer	-2.46 ± 0.07	-2.5 ± 0.2	-2.5 ± 0.1	-2.2 ± 0.2
PDF scaling exponent n for	winter	-2.75 ± 0.09	-2.41 ± 0.05	-2.9 ± 0.1	-3.23 ± 0.09
shear $\dot{\tau}$	summer	-2.77 ± 0.07	-2.4 ± 0.2	-2.4 ± 0.1	-3.0 ± 0.1

S-2 Example Maps of Divergence, Vorticity, and Shear

In Section 3.1 maps of divergence, vorticity, and shear for November 1999 are presented as an example. Here more examples are presented for different years and seasons. For these examples the filter from Bouillon and Rampal (2015) was applied.

S-2.1 Divergence

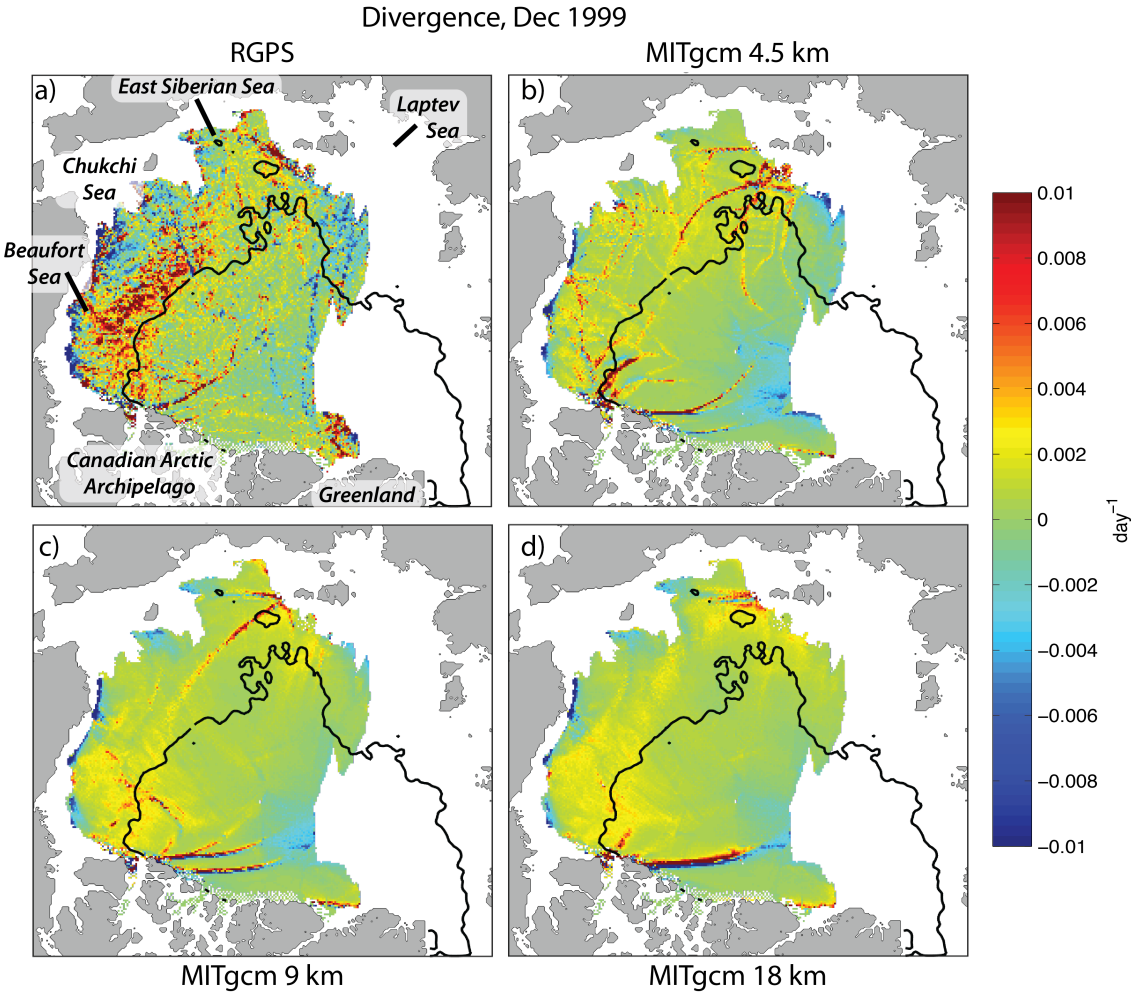

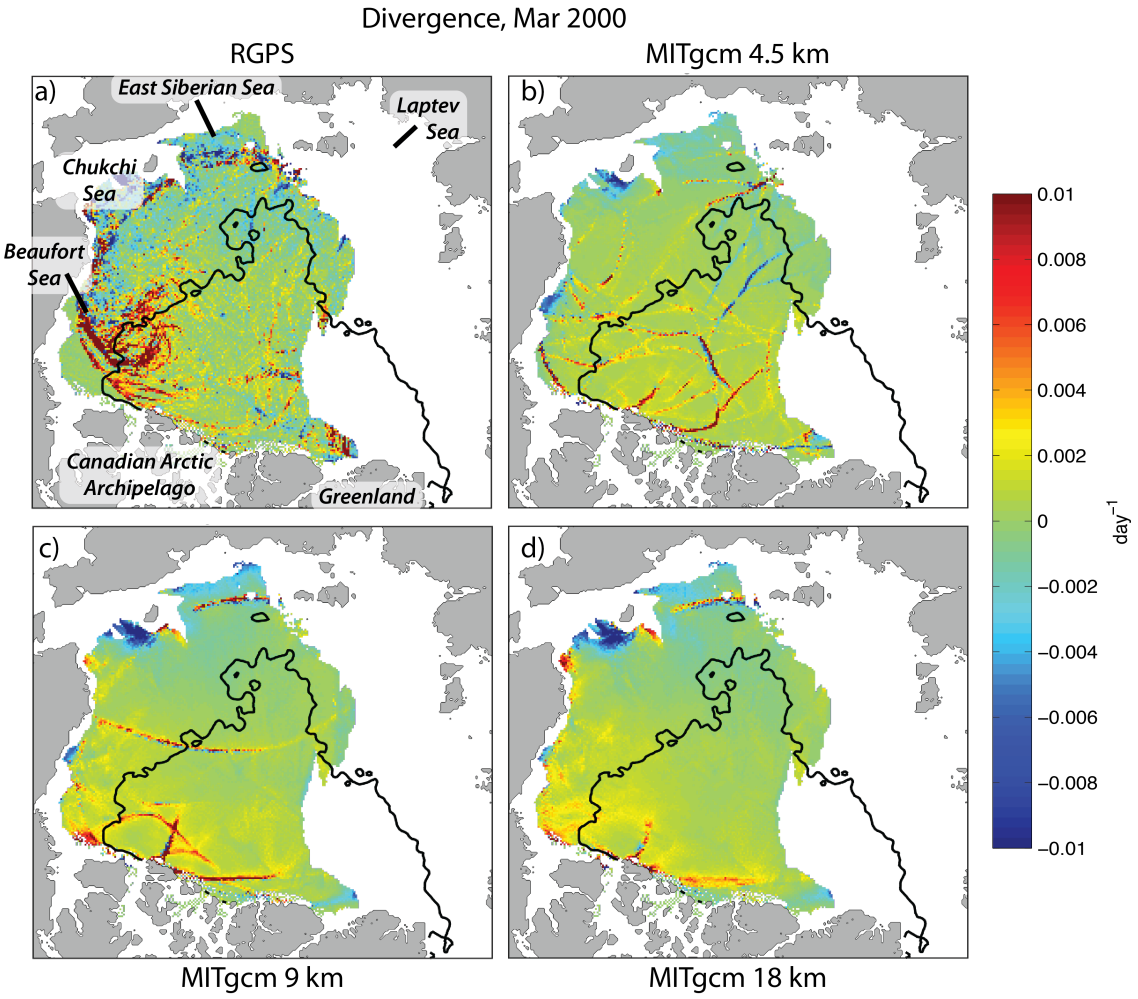
Divergence, Mar 2000
RGPS
MITgcm 4.5 km
a)
b)
East Siberian Sea
Laptev Sea
Chukchi Sea
Beaufort Sea
Canadian Arctic Archipelago
Greenland
c)
d)
MITgcm 9 km
MITgcm 18 km
0.01
0.008
0.006
0.004
0.002
0
−0.002
−0.004
−0.006
−0.008
−0.01
day^{-1}

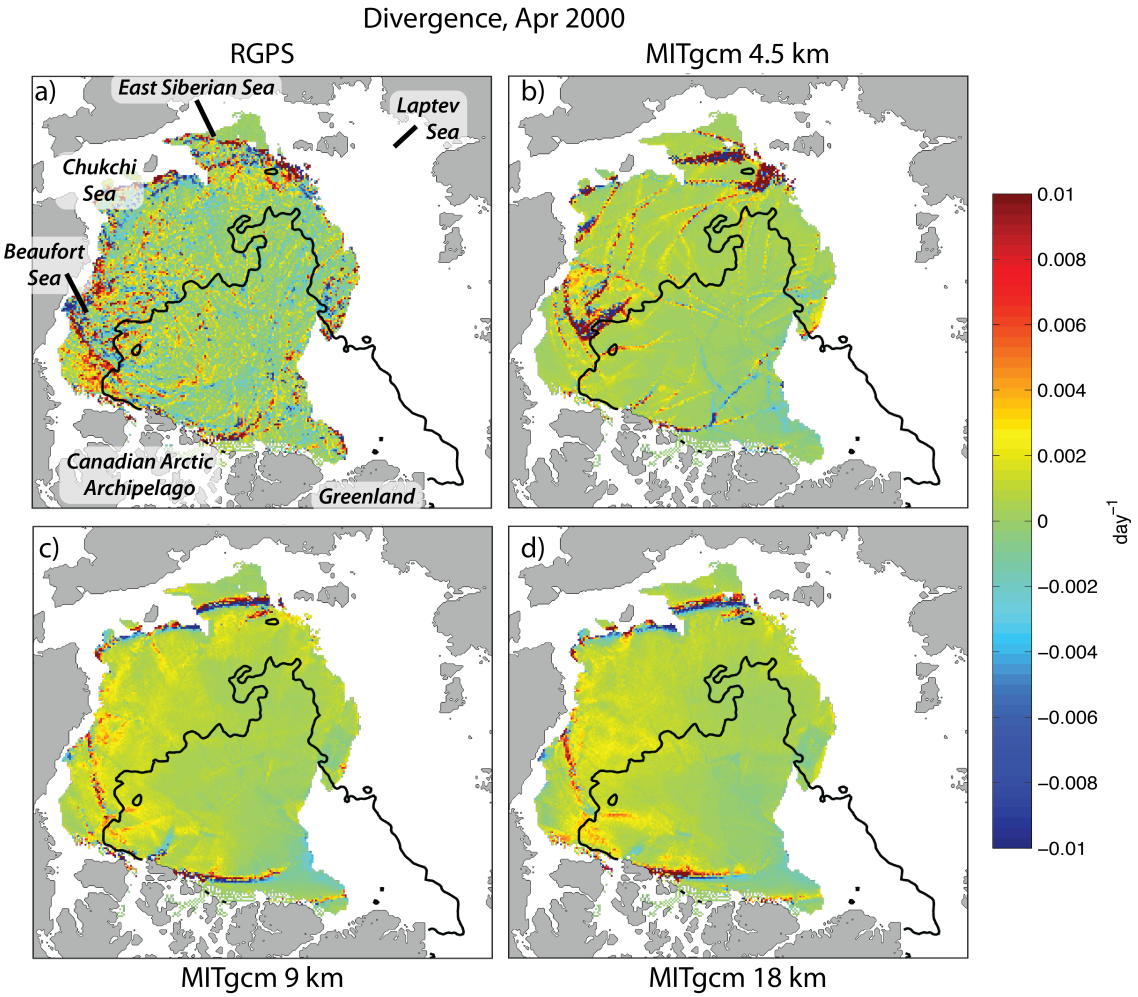
Divergence, Apr 2000
RGPS
MITgcm 4.5 km
a)
b)
East Siberian Sea
Laptev Sea
Chukchi Sea
Beaufort Sea
Canadian Arctic Archipelago
Greenland
c)
d)
MITgcm 9 km
MITgcm 18 km
0.01
0.008
0.006
0.004
0.002
0
−0.002
−0.004
−0.006
−0.008
−0.01
day^{-1}

S-2.2 Vorticity

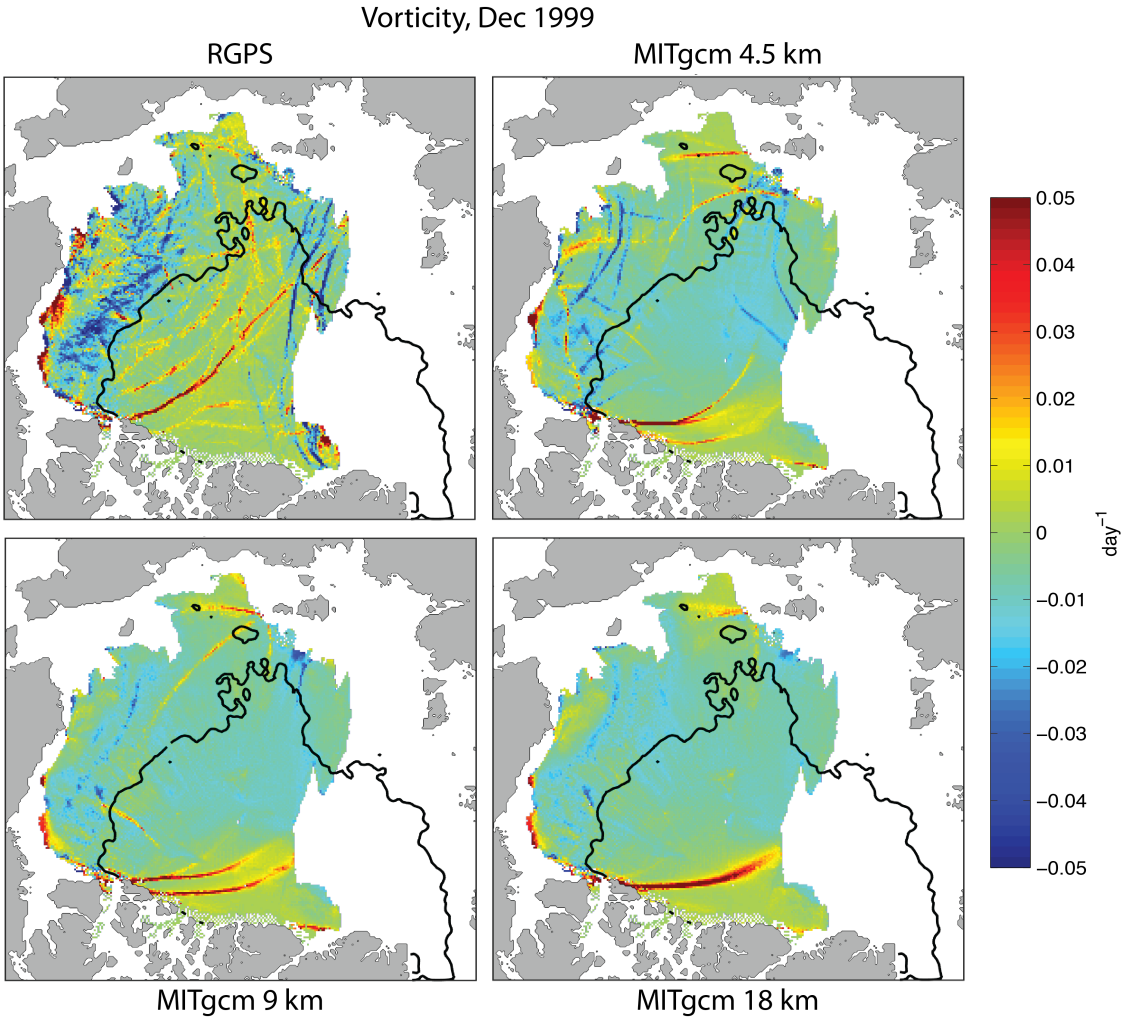

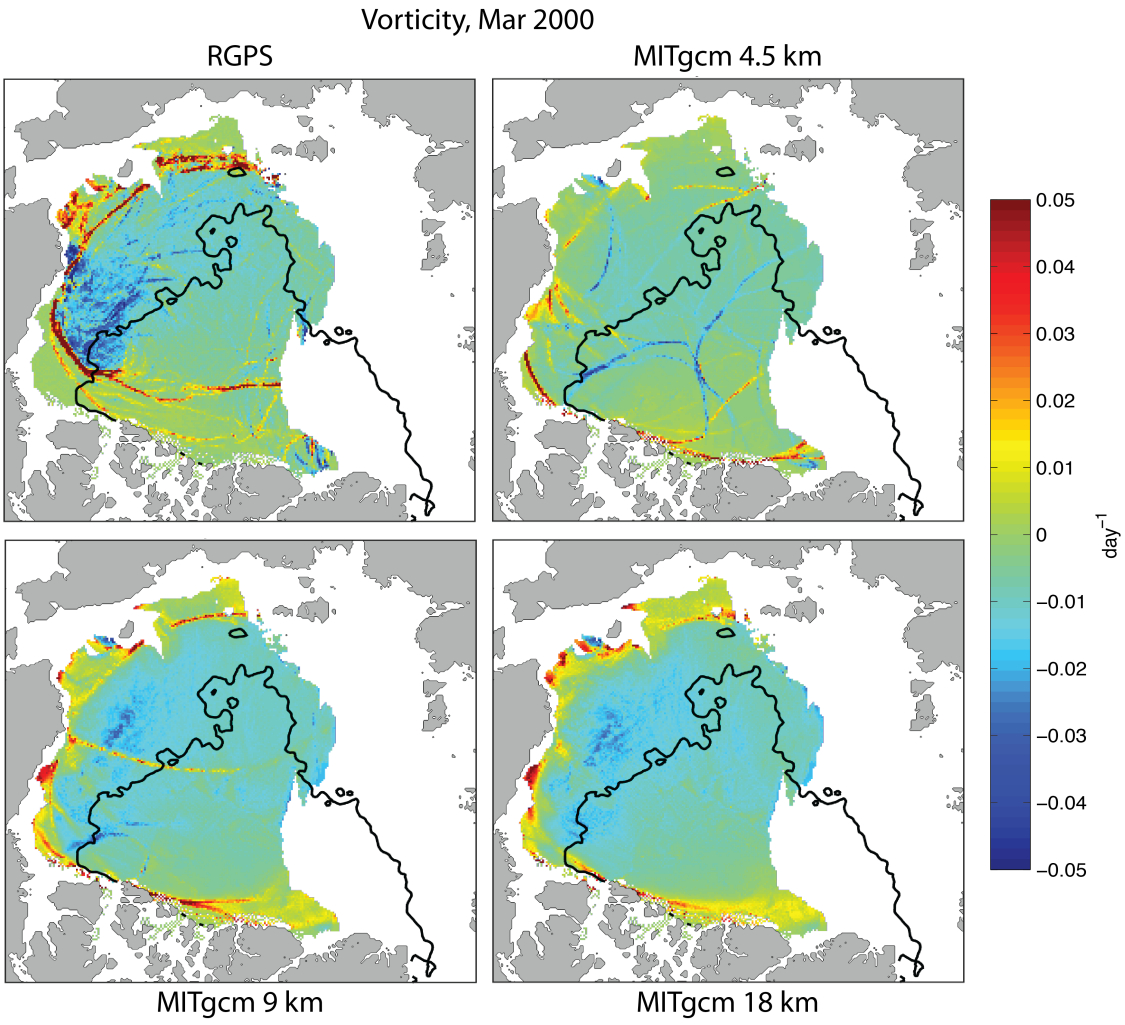
Vorticity, Mar 2000
RGPS
MITgcm 4.5 km
MITgcm 9 km
MITgcm 18 km
0.05
0.04
0.03
0.02
0.01
0
−0.01
−0.02
−0.03
−0.04
−0.05
day^{-1}

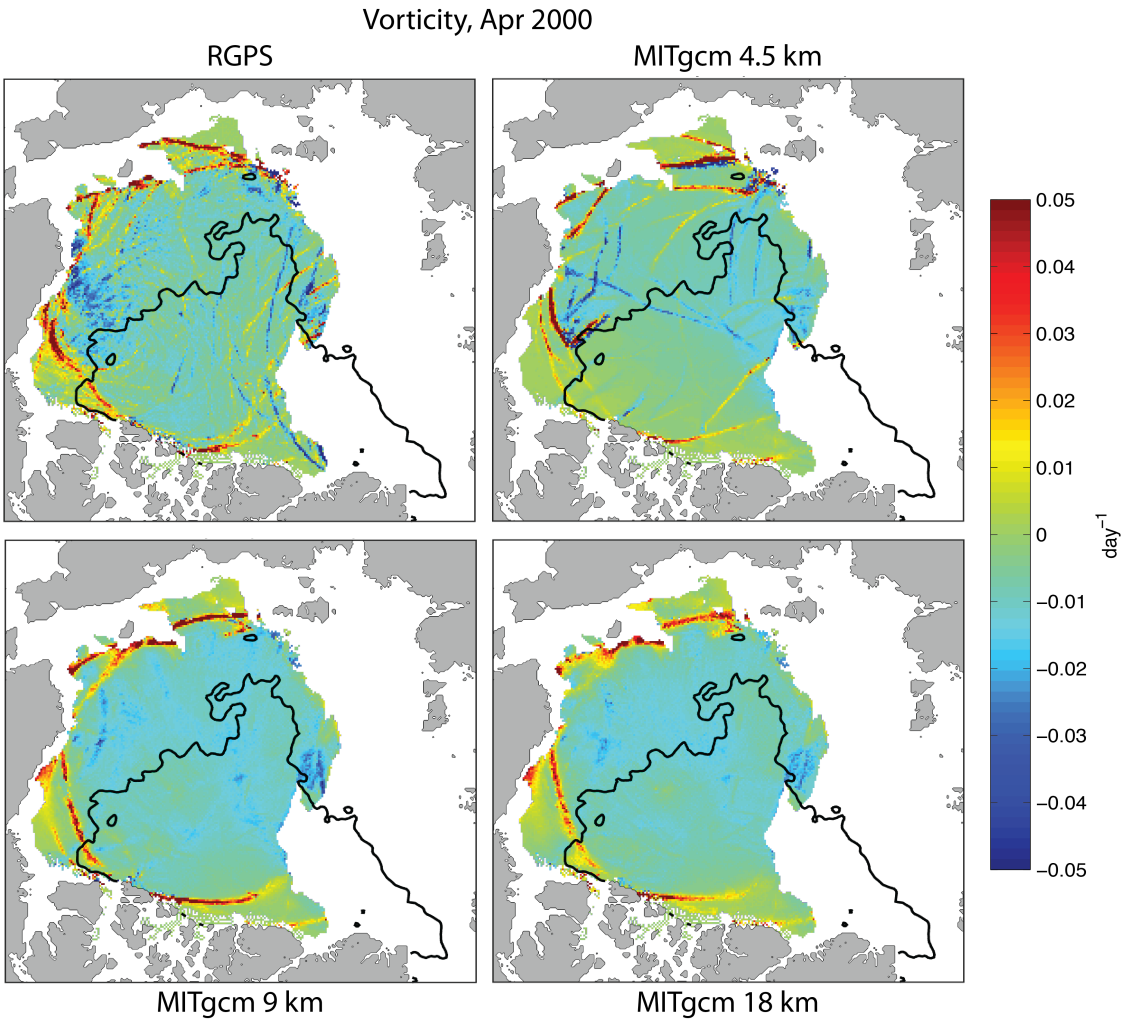
Vorticity, Apr 2000
RGPS
MITgcm 4.5 km
MITgcm 9 km
MITgcm 18 km
0.05
0.04
0.03
0.02
0.01
0
−0.01
−0.02
−0.03
−0.04
−0.05
day^{-1}

S-2.3 Shear

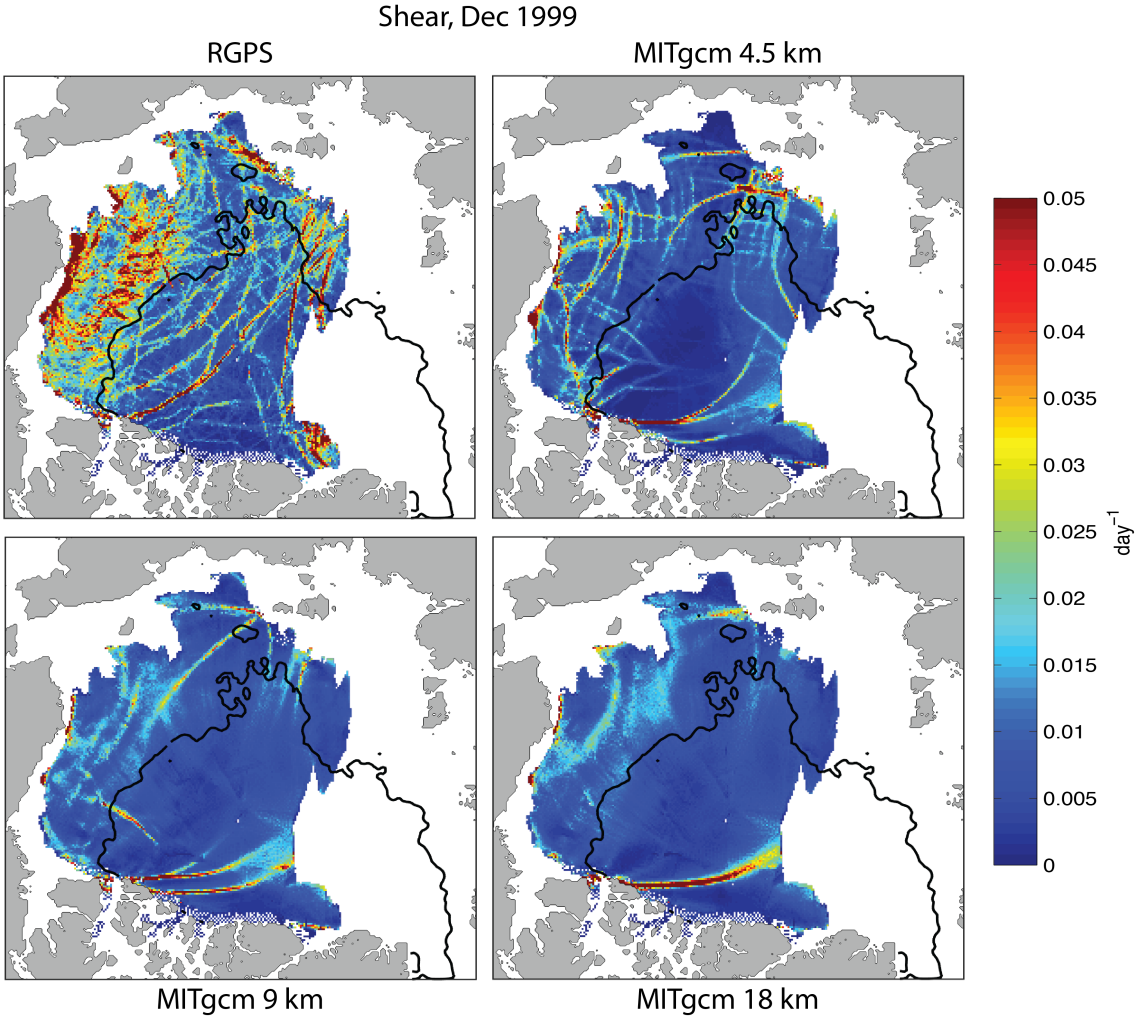
Shear, Dec 1999
RGPS
MITgcm 4.5 km
MITgcm 9 km
MITgcm 18 km
0.05
0.045
0.04
0.035
0.03
0.025
0.02
0.015
0.01
0.005
0
day^{-1}

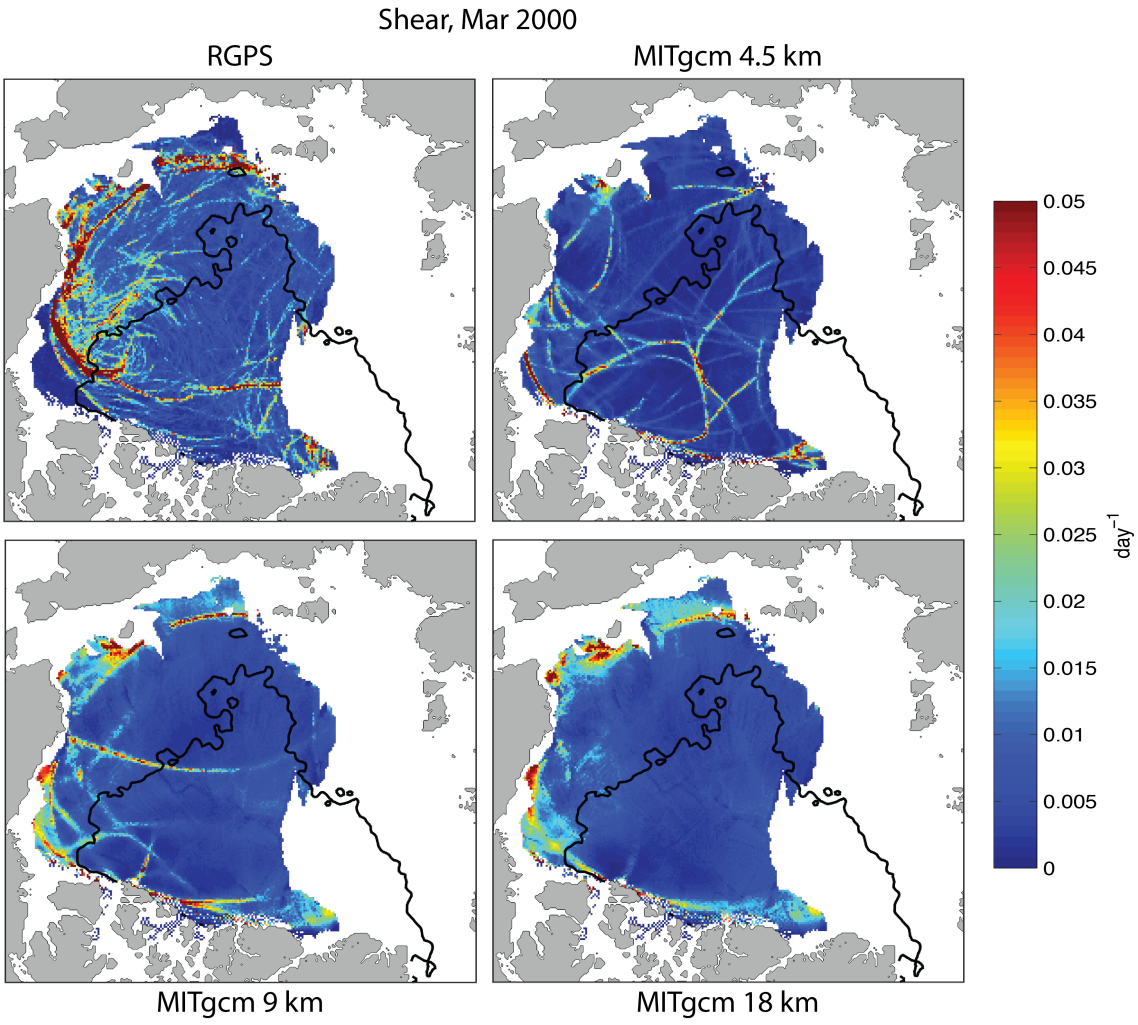
Shear, Mar 2000
RGPS
MITgcm 4.5 km
MITgcm 9 km
MITgcm 18 km
0.05
0.045
0.04
0.035
0.03
0.025
0.02
0.015
0.01
0.005
0
day^{-1}

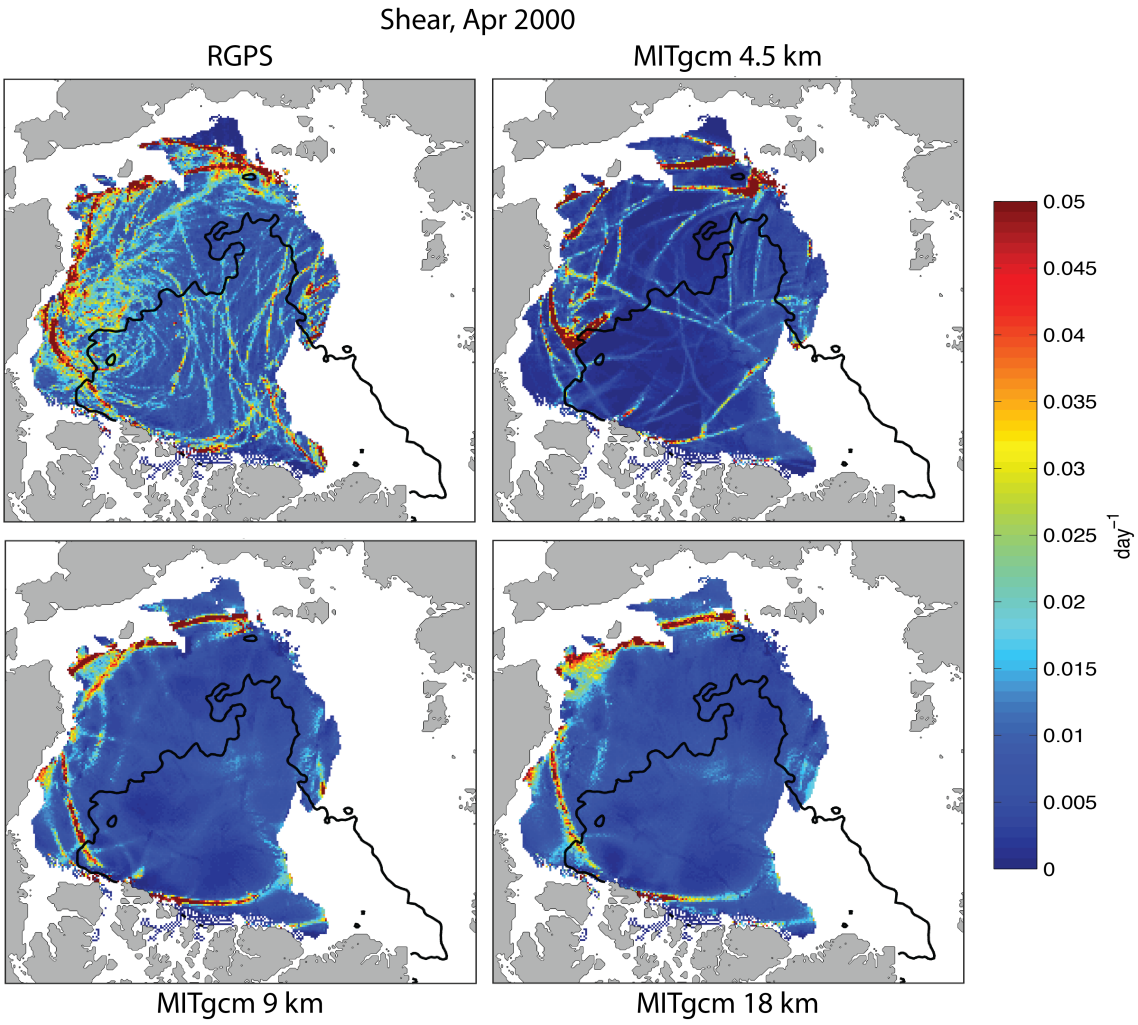

References

Bouillon, S. and Rampal, P.: On producing sea ice deformation data sets from SAR-derived sea ice motion, The Cryosphere, 9, 663–673, doi:10.5194/tc-9-663-2015, http://www.the-cryosphere.net/9/663/2015/, 2015.